

# Emergence of Metachronal Waves in Active Microtubule Arrays

Stephen E Martin,<sup>1</sup> Matthew E Brunner,<sup>2</sup> and Joshua M Deutsch<sup>1,\*</sup>

<sup>1</sup>*Department of Physics, University of California, Santa Cruz, CA 95064, USA*

<sup>2</sup>*Voltaic Inc. 2150 Shattuck Ave, #704 Berkeley, CA 94704*

(Dated: May 31, 2021)

The physical mechanism behind the spontaneous formation of metachronal waves in microtubule arrays in a low Reynolds number fluid has been of interest for the past several years, yet is still not well understood. We present a model implementing the hydrodynamic coupling hypothesis from first principles, and use this model to simulate kinesin-driven microtubule arrays and observe their emergent behavior. The results of simulations are compared to known experimental observations by Sanchez et al.[1, 2]. By varying parameters, we determine regimes in which the metachronal wave phenomenon emerges, and categorize other types of possible microtubule motion outside these regimes.

Metachronal waves refer to the synchronization of thin, flexible appendages that result in large-scale wavelike formations. These appear in biological systems at the macroscopic scale (e.g. the motion of millipede legs) and at the microscopic scale (e.g. cilia in air pathways). On the microscopic level, metachronal waves are essential components of several critical biological processes, from motility in microorganisms to mucus clearance in human bronchial tubes [3, 4]. If cilia are unable to effectively move and synchronize, the results are often severe – especially if the disorder is genetic [3]. Research into physical explanations for cilia beating [5], and of spontaneous metachronal behavior in cilia is ongoing and still not well understood [6, 7], although many have suggested that this phenomenon can be explained from hydrodynamic coupling between cilia [8–11].

Recently, in some remarkable experiments, Sanchez et al. demonstrated metachronal wave behavior in an *in vitro* system[1, 2]. Microtubules (MTs) aggregated into bundles of length 10 – 100 $\mu$ m due to the addition of polyethylene glycol [12]. Many of these bundles attached at one end to a fixed boundary forming dense arrays. When exposed to a solution containing clusters of kinesin and ATP, sustained metachronal wave behavior between MT bundles (similar to that displayed by cilia and flagella) was observed. MT bundles were constrained to move between two glass slides. It is surprising that a system with such few ingredients could develop complex behavior that so closely resembles biological systems, which are made up from a much more complicated machinery. Proteomic analysis indicate that eukaryotic cilia are composed of many hundreds of proteins [13].

Some important details of this *in vitro* system are still unclear, most notably whether the MTs in this experiment are unipolar or of mixed polarity. Opposite polarity MTs will move past each other, causing separation into unipolar bundles [14, 15]. We present analytical and numerical arguments for unipolarity in S-IV. The surprising mechanism for the motion of unipolar bundles described here, has not previously been given [1, 2], and we believe that the agreement between our model and experiments

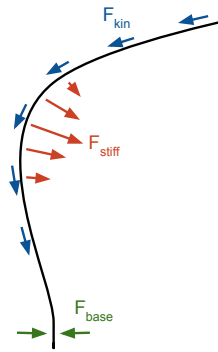


FIG. 1. Conceptual illustration of forces acting on a single polymer that are not due to hydrodynamic interactions. The blue vectors indicate the buckling forces due to kinesin walkers (tangent to polymer), the red vectors show the direction and relative magnitude of stiffness forces (in the direction of  $d^4\mathbf{r}/ds^4$ ), and the green arrows indicate a restorative force keeping the base of the polymer approximately perpendicular to the binding surface.

provides further evidence to support our proposed explanation.

The general mechanism proposed is quite similar to the model used to describe and simulate cytoplasmic streaming in *Drosophila* oocytes, and the fact that it can be adapted as such is in many ways a testament to its predictive power. A fair amount of attention has been paid in recent years to the understanding of how metachronal waves form in such arrays [16–19]. However, such models often rely on assumptions about individual MT (or cilia) beat patterns and/or on phenomenology. The model we propose makes no such assumptions (beyond some minor simplifications), relying on first-principles fluid mechanics calculations. This is important, as it is not clear why one would want additionally to impose oscillatory behavior on individual MTs given the lack of a well defined internal structure.

We now present a model for the simulation of the Sanchez et al. system. A similar method has been used successfully to simulate cytoplasmic streaming in *Drosophila* oocytes[20], and is based on theoretical work completed several decades ago regarding the calculation of Stokes flows created by a point force (stokeslet) near no-slip boundaries[21, 22]. A conceptual explanation of this mechanism is given below, and further details regarding theory and implementation are given in supplementary materials S-II and S-III.

An illustration of how MT bundles are simulated is given in Fig. 1. Each MT bundle is modeled as a chain of monomers (i.e. polymer) which are held an approximately fixed distance from one another by a spring force. The base of each polymer is anchored to a single point, and the polymer at the base is kept roughly perpendicular to the anchoring surface. Let the polymer be described by the curve  $\mathbf{r}(s)$ , where  $\mathbf{r}(0)$  is the location of the polymer base, and  $s$  is the arc length. We give the polymer a stiffness by implementing an energetic cost of bending proportional to curvature squared, which implies a local force at  $s$  proportional to  $d^4\mathbf{r}/ds^4$ . Additionally, monomers feel a “buckling” force due to the drag from the walking kinesin  $F_{kin} = -f_k d\mathbf{r}/ds$ , which is parallel to the polymer and toward the polymer base.  $f_k$  will depend linearly on the speed of the kinesin and the solvent viscosity. This force continually adds energy to the system (making it active), and has been shown to be a good representation of the average drag force due to kinesin walking along the microtubule away from the polymer base [20].

This kind of model for a single chain was first employed to understand glide assay dynamics in two dimensions [23]. In three dimensions, periodic waves develop whose dynamics have been analyzed in detail [20], and related theoretical work has recently also been performed [24]. However, scaling can be used to get the relevant length and timescales [23]. The average radius of curvature depends on the strength of the buckling force  $f_k$ , and the elastic constant of a filament characterizing its stiffness  $k_{stiff}$ . The radius of curvature over quite a wide range of parameters can be shown to be  $R = (k_{stiff}/(\beta f_k))^{1/3}$ , where  $\beta \approx 0.05$ . Likewise, the angular frequency is  $\omega = f_k/(\nu R)$ , where  $\nu$  is the hydrodynamic drag coefficient per unit length. Although there is a fairly large experimental uncertainty in parameters used to model a *Drosophila* oocyte, this model finds quite good agreement with the experimental time and length scales.  $R$  was predicted to be  $25 - 54\mu\text{m}$ , close to the  $16.3 \pm 2.2\mu\text{m}$  observed. Likewise, the time scale was predicted to be  $203 - 1094\text{s}$ , which is in the observed range of  $370 \pm 42\text{s}$ . It is interesting that the length and time scales observed by Sanchez et al. are also quite close to these numbers, and that the frequency of biological cilia beating is often three orders of magnitude higher than this.

Polymers also feel hydrodynamic forces. As the force from the kinesin causes the polymers to buckle, we begin to see complex motion. Each monomer acts as a point force (stokeslet) in the surrounding fluid. This force, that a monomer exerts on the fluid, is simply the sum of all of the other forces on the monomer: because the Reynolds number is nearly zero, there are no inertial terms, meaning the force is transferred perfectly from the monomer to the fluid. As this is a Stokes flow, the flow contributions from all stokeslets add linearly, and we can (in principle) calculate the flow everywhere. However, we only need to calculate the fluid velocity at points with monomers. Therefore, the evolution can be calculated via a pairwise sum over all monomers (see the supplemental materials S-II).

We also assume all polymer motion is two dimensional with a constant value of  $z$ , which is physically sensible when considering the geometry of the Sanchez et al. experiments. In this experiment, MT bundles were observed between glass slides, with a height  $H$ , of approximately  $10\mu\text{m}$ , creating a narrow channel for which fluid can flow. For this reason, we adopt a two dimensional geometry. In addition, the no-slip boundaries of the plates have a large impact on the hydrodynamic forces between monomers[21, 22], which we give explicitly in the supplemental materials S-II. Other close-range contact forces were also used (repulsion from anchoring surface, monomer-monomer repulsion), and these are explained in the supplementary materials S-III.

We can now address at the qualitative level the mechanism by which we propose the metachronal waves observed by Sanchez et al. form. As kinesin walk away from the polymer bases, the polymers will tend to buckle. If a polymer is isolated, this buckling will lead to corkscrew motion or periodic waves[20]. When placed in an array, however, nearby polymers will exert hydrodynamic forces on one another that tend to synchronize their motion. If these hydrodynamic forces are sufficiently strong, this can cause a transition from disordered motion to aligned MTs and correlated motion.

Despite the fact that this model was developed to explain and simulate cytoplasmic streaming, its mechanism can be easily adapted for related biological phenomena. Indeed, when the conditions of the Sanchez et al. experiment are simulated in the same way, we observe metachronal waves. It is not clear if this is formally a transition or a more continuous crossover effect, but the results found make strong predictions that should be testable experimentally. In the following, we present the results of these simulations and discuss the required conditions for metachronal wave formation.

Videos of select simulations are included in the Supplementary Materials. Fig. 2 shows some still frames of simulated arrays demonstrating metachronal wave behavior in both the planar and circular geometries.

We characterize the behavior of each system using the

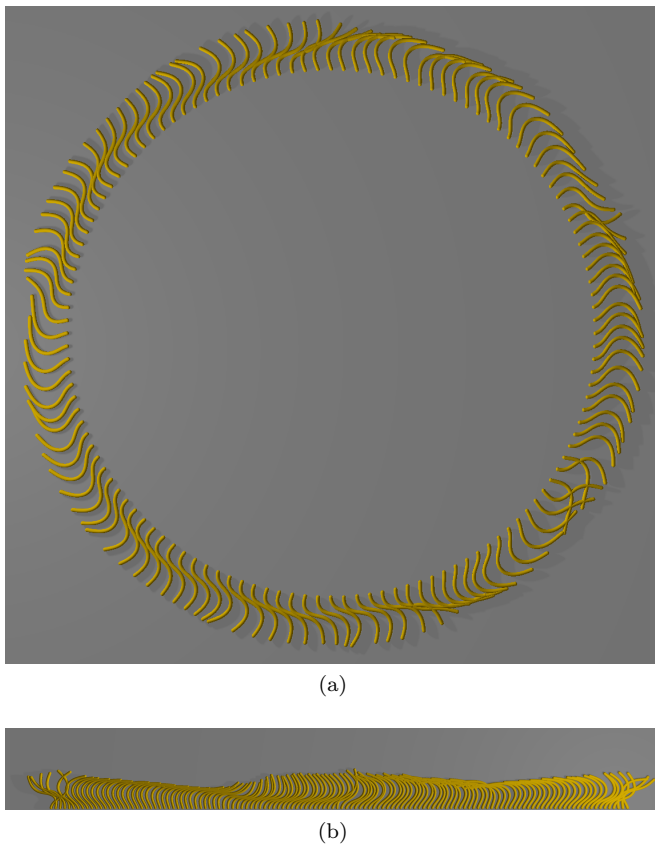


FIG. 2. Simulated metachronal wave formation for 128-polymer arrays in (a) circular and (b) planar geometries. In both cases,  $k_{oseen} = 0.1$ ,  $k_{stiff} = 10.0$ ,  $H = 1$ .

correlation function for the chain ends  $x(i, t)$ ,

$$C(\Delta i, \Delta t) = \langle \Delta x(i + \Delta i, t + \Delta t) \Delta x(i, t) \rangle, \quad (1)$$

where

$$\Delta x(i, t) = x(i, t) - \langle x(i, t) \rangle.$$

The average is performed over all chain indices  $i$ , and time  $t$ , after a period of equilibration. Figs. 3, 4, and 5 show correlation functions for planar and a circular geometries (for the circular geometry, the polar angle  $\theta$  is the position variable rather than  $x$ ). In the following, we will discuss these and examine how the system responds to changes in the strength of the interaction tensor,  $k_{oseen}$ ,  $k_{stiff}$ , and height  $H$ . It should be noted that changes in the viscosity or kinesin velocity and density (that affect  $f_k$ ), can be absorbed into a rescaling of time, and of  $k_{stiff}$ .

$k_{oseen}$ , has a dramatic effect on the type of wave behavior seen, or whether it is observed at all. This strength is a function of the hydrodynamic effects of kinesin walking along microtubules, and will depend on their density and speed, as explained in detail in Ref. [20]. Fig. 3 shows the correlation results of three 128-polymer simulations in the same circular geometry shown in Fig. 2(a)

for three different values of  $k_{oseen}$ . There is an overall strengthening of the metachronal behavior as  $k_{oseen}$  is increased from 0.1 to 0.2. The sign of the slope reflects the initial conditions of the system. Long lived waves travel predominantly in a single direction over long times scales resulting in a slope of the crests of the correlation function that can either be positive or negative. Similar crests are seen in the analysis of the real experimental data [1]. With this circular geometry, the correlation function must be periodic, which is why it rises again when  $i$  becomes large.

The polymer stiffness  $k_{stiff}$  also has an interesting effect on metachronal wave formation. Fig. 4 shows the correlation functions for  $k_{stiff} = 5.0$ , 10.0, and 20.0 in a planar geometry. While Figs. 4(a-b) are qualitatively similar, we do see an apparent decrease in the metachronal wavelength. Figs. 4(c-d) show that if the polymer is made too stiff, no metachronal behavior is observed at all. In general, planar geometry appears to cause more coherence in the motion of the different bundles, and the correlation function is dominated by motion at the longest lengths and time scales.

The distance between plates,  $H$ , has a considerable effect on the dynamics as well. Longer range, more coherent motion is observed when  $H$  is larger, and short range, less coherent motion when  $H$  is small. See Fig. 5. This is to be expected due to the strong screening effect that these boundary conditions impose. Smaller  $H$  reduces the hydrodynamic coupling, causing a decrease in coherence.

When comparing these results to those of Sanchez et al., we find that the basic features agree. The videos included in the supplemental materials qualitatively mimic the experimental videos, and the experimental correlation analysis agrees quite well with the simulations. More importantly, this agreement between theory and experiment was reached from first principles. We only use a handful of forces in our simulations, and each force has a physical justification for being used.

There are potential shortcomings of this model that may result in some differences between experiment and theory. The first is that the experiments observe bundles of microtubules that taper away from their base. The hydrodynamics are not expected to be uniform along the length of a chain. In addition these bundles will, for short enough times, behave like rigid material, but for longer times, because they are connected through walking kinesin molecules, will behave more as individual microtubules with a greatly reduced elastic constant. On the time scales of the motion, we expect to be in the latter regime. However the details of the hydrodynamics and elasticity in these bundles is still not understood experimentally. In fact, as we mentioned earlier, the polarity of individual MT's is not known experimentally, and arguments for their unipolarity are given in the supplementary information, S-IV. But still, the basic mechanism of

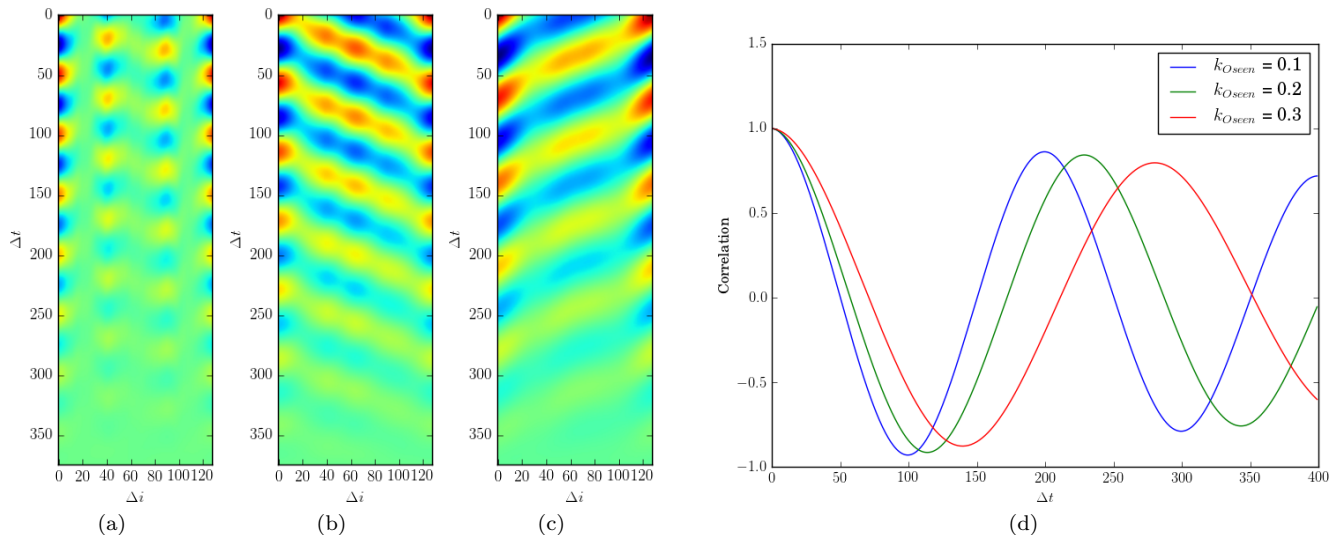


FIG. 3. Full correlation functions for circular geometry with  $H = 1$  and  $k_{stiff} = 10$ , with  $k_{osen} = 0.1, 0.2$ , and  $0.3$  (a-c, respectively). The correlation function at  $\Delta i = 0$  for all of these values of  $k_{osen}$  are shown in (d).

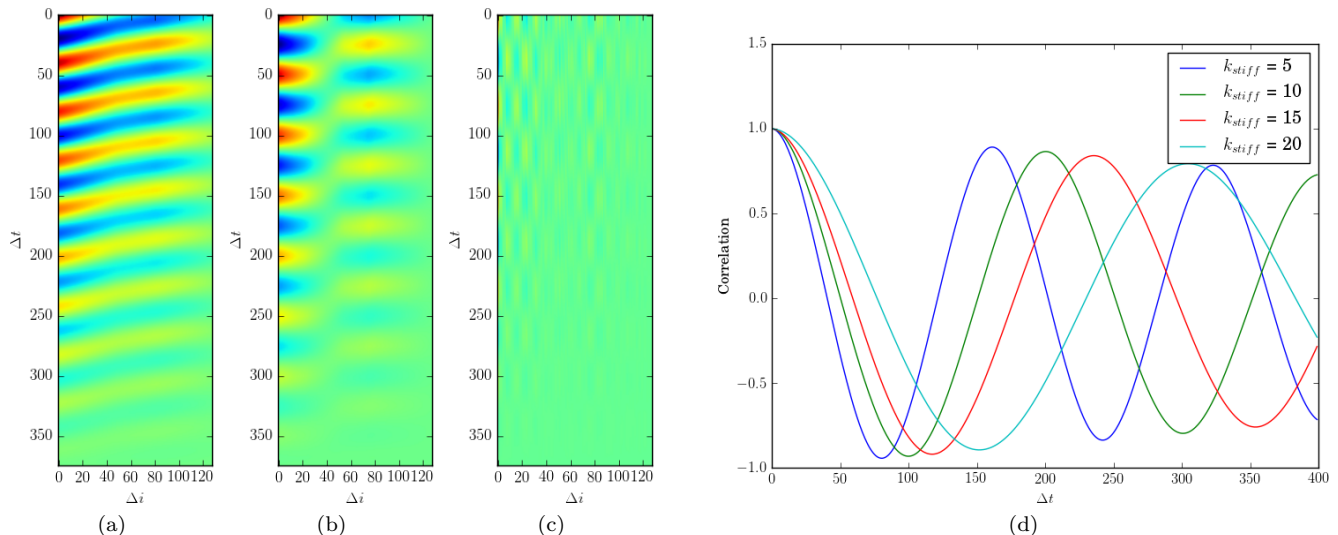


FIG. 4. Full correlation functions for planar geometry with  $H = 1$  and  $k_{osen} = 0.1$ , with  $k_{stiff} = 5.0, 10.0$ , and  $20.0$  (a-c, respectively). The correlation function at  $\Delta i = 0$  for all of these values of  $k_{stiff}$  are shown in (d).

dynamic buckling due to kinesin drag, and metachronal waves being generated by hydrodynamic coupling, is robust over a wide parameter range, so we believe that these complications, aside from unipolarity, will not alter the basics of our explanation.

At a more technical level, there are other things that may make a slight difference to the results here. The bundles are constrained to move only in the  $xy$ -plane, and while it is true that MT motion is nearly 2-dimensional, there is some room in the  $z$ -direction that MT bundles can occupy. Additionally, this model does not account for the fluid boundary condition at the anchoring surface. This may introduce some errors if a monomer becomes

close ( $\sim H$ ) to the anchoring plane. However, because of the screening effects of the plates, this should not alter the behavior at distances large compared to the plate separation. We have tested for this by adding image charges to the planar case, and found that their effects on correlations are small, as expected.

In conclusion, we have developed a model for the spontaneous formation of wavelike behavior in active polymer arrays that only requires two ingredients: semi-flexible chains tethered to a surface, and motors walking from their bases to their tips. The hydrodynamics in their confined geometry gives rise to metachronal waves that appear remarkably similar to what is observed experi-

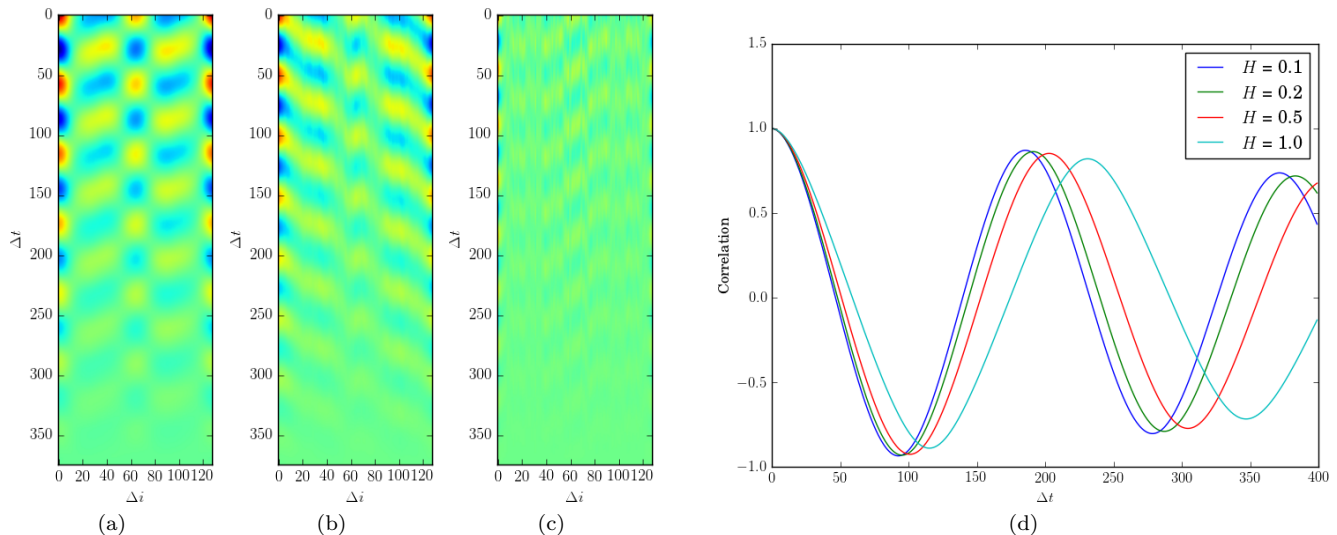


FIG. 5. Full correlation functions for circular geometry with  $k_{stiff} = 10$ ,  $k_{osseen} = 0.2$ , and  $H = 1.0, 0.5$ , and  $0.1$  (a-c, respectively). The correlation function at  $\Delta i = 0$  for all of these values of  $H$  are shown in (d).

mentally [1, 2]. There is no need to posit additional mechanisms that force individual bundles to oscillate. This all happens as a consequence of Newton's laws and fluid mechanics, allowing us to gain a better understanding of how metachronal waves form with considerable predictive power. As such, we have examined new parameter spaces and have demonstrated boundaries between different types of metachronal behavior and regimes in which no metachronal behavior exists. It would be of great interest to test these predictions experimentally. Given the simplicity and robust nature of this mechanism, and the ubiquity of microtubules and kinesin in cells, it gives one further impetus to look for other places in biology where this kind of behavior can be found.

J.M.D. thanks Bill Saxton, Itamar Kolvin, Alex Tayar, and Zvonimir Dogic for useful discussions. S.E.M. was partially supported by the ARCS Foundation. This work was also supported by the Foundational Questions Institute <<http://fqxi.org>>.

\* [josh@ucsc.edu](mailto:josh@ucsc.edu)

- [1] T. Sanchez, D. Welch, D. Nicastro, and Z. Dogic, *Science* **333**, 456 (2011).
- [2] T. Sanchez and Z. Dogic, in *Methods in enzymology*, Vol. 524 (Elsevier, 2013) pp. 205–224.
- [3] B. A. Afzelius, *J. Pathol.* **204**, 470 (2004).
- [4] Y. Okada, S. Takeda, Y. Tanaka, J., C. I. Belmonte, and N. Hirokawa, *Cell* **121**, 633 (2005).
- [5] C. J. Brokaw, *Proceedings of the National Academy of Sciences* **72**, 3102 (1975).
- [6] S. Camalet, F. Jülicher, and J. Prost, *Physical Review Letters* **82**, 1590 (1999).
- [7] C. B. Lindemann and K. A. Lesich, *J Cell Sci* **123**, 519 (2010).
- [8] M. A. Sleight, *Int. Rev. Cytol.* **25**, 31 (1969).
- [9] M. A. Sleight, ed., *Cilia and Flagella* (Academic Press, 1974).
- [10] L. Gheber and Z. Priel, *Biophys. J.* **55**, 183 (1989).
- [11] S. Gueron, K. Levit-Gurevich, N. Liron, and J. J. Blum, *Prot. Natl. Acad. Sci. USA* **94**, 6001 (1997).
- [12] D. J. Needleman, M. A. Ojeda-Lopez, U. Raviv, K. Ewert, J. B. Jones, H. P. Miller, L. Wilson, and C. R. Safinya, *Physical review letters* **93**, 198104 (2004).
- [13] G. J. Pazour, N. Agrin, J. Leszyk, and G. B. Witman, *J Cell Biol* **170**, 103 (2005).
- [14] K. Kruse and F. Jülicher, *Physical Review Letters* **85**, 1778 (2000).
- [15] T. B. Liverpool and M. C. Marchetti, *Physical Review Letters* **90**, 138102 (2003).
- [16] M. C. Lagomarsino, P. Jona, and B. Bassetti, *Phys. Rev. E* **68**, 021908 (2003).
- [17] B. Guirao and J.-F. Joanny, *Biophysical journal* **92**, 1900 (2007).
- [18] J. Elgeti and G. Gompper, *Proceedings of the National Academy of Sciences* **110**, 4470 (2013).
- [19] T. Niedermayer, B. Eckhardt, and P. Lenz, *Chaos: An Interdisciplinary Journal of Nonlinear Science* **18**, 037128 (2008).
- [20] C. E. Monteith, M. E. Brunner, I. Djagaeva, A. M. Bielecki, J. M. Deutsch, and W. M. Saxton, *Biophys. J.* **110**, 2053 (2016).
- [21] J. R. Blake, *Mathematical Proceedings of the Cambridge Philosophical Society* **70**, 303 (1971).
- [22] N. Liron and S. Mochon, *Journal of Engineering Mathematics* **10**, 287 (1976).
- [23] L. Bourdieu, T. Duke, M. Elowitz, D. Winkelmann, S. Leibler, and A. Libchaber, *Physical Review Letters* **75**, 176 (1995).
- [24] G. De Canio, E. Lauga, and R. E. Goldstein, *Journal of The Royal Society Interface* **14**, 20170491 (2017).

# Supplementary materials to: Emergence of Metachronal Waves in Active Microtubule Arrays

Stephen E Martin,<sup>1</sup> Matthew E Brunner,<sup>2</sup> and Joshua M Deutsch<sup>1,\*</sup>

<sup>1</sup>*Department of Physics, University of California, Santa Cruz, CA 95064, USA*

<sup>2</sup>*Voltaic Inc. 2150 Shattuck Ave, #704 Berkeley, CA 94704*

(Dated: May 31, 2021)

arXiv:1806.06993v1 [q-bio.SC] 19 Jun 2018

---

\* [josh@ucsc.edu](mailto:josh@ucsc.edu)

## I. SUPPLEMENTARY VIDEO LEGENDS

Videos at <https://sites.google.com/ucsc.edu/joshdeutsch/metachronal-videos?authuser=0>

**Supplementary video S1:** 128 microtubule bundles (length 16) with kinesin walkers in a circular geometry in a fluid chamber with  $k_{\text{seen}} = 0.1$ , chamber height  $H = 1.0$ ,  $k_{\text{stiff}} = 10$ .

**Supplementary video S2:** 128 microtubule bundles (length 16) with kinesin walkers in a circular geometry in a fluid chamber with  $k_{\text{seen}} = 0.2$ , chamber height  $H = 0.1$ ,  $k_{\text{stiff}} = 10$ .

**Supplementary video S3:** 128 microtubule bundles (length 16) with kinesin walkers in a circular geometry in a fluid chamber with  $k_{\text{seen}} = 0.2$ , chamber height  $H = 0.2$ ,  $k_{\text{stiff}} = 10$ .

**Supplementary video S4:** 128 microtubule bundles (length 16) with kinesin walkers in a circular geometry in a fluid chamber with  $k_{\text{seen}} = 0.2$ , chamber height  $H = 0.5$ ,  $k_{\text{stiff}} = 10$ .

**Supplementary video S5:** 128 microtubule bundles (length 16) with kinesin walkers in a circular geometry in a fluid chamber with  $k_{\text{seen}} = 0.2$ , chamber height  $H = 1.0$ ,  $k_{\text{stiff}} = 10$ .

**Supplementary video S6:** 128 microtubule bundles (length 16) with kinesin walkers in a circular geometry in a fluid chamber with  $k_{\text{seen}} = 0.3$ , chamber height  $H = 1.0$ ,  $k_{\text{stiff}} = 10$ .

**Supplementary video S7:** 128 microtubule bundles (length 16) with kinesin walkers in a planar geometry in a fluid chamber with  $k_{\text{seen}} = 0.1$ , chamber height  $H = 1.0$ ,  $k_{\text{stiff}} = 5$ .

**Supplementary video S8:** 128 microtubule bundles (length 16) with kinesin walkers in a planar geometry in a fluid chamber with  $k_{\text{seen}} = 0.1$ , chamber height  $H = 1.0$ ,  $k_{\text{stiff}} = 10$ .

**Supplementary video S9:** 128 microtubule bundles (length 16) with kinesin walkers in a planar geometry in a fluid chamber with  $k_{\text{seen}} = 0.1$ , chamber height  $H = 1.0$ ,  $k_{\text{stiff}} = 15$ .

**Supplementary video S10:** 128 microtubule bundles (length 16) with kinesin walkers in a planar geometry in a fluid chamber with  $k_{\text{seen}} = 0.1$ , chamber height  $H = 1.0$ ,  $k_{\text{stiff}} = 20$ .

**Supplementary video S11:** 2 microtubules of opposite polarities, green MT's have minus ends on surface, and blue MT's have plus ends on the surface. There are fixed boundary conditions on the surface. This shows a simulation for a set of parameters where the two microtubules move. This behavior was never found when there were more than 2 microtubules in a bundle.

**Supplementary video S12:** Pillar of 9 microtubules of opposite polarities, green MT's have minus ends on surface, and blue MT's have plus ends on the surface. There are sliding boundary conditions on the surface. This shows a simulation in a regime with sufficiently weak attractive interactions,  $f_a = 1$ , where there is a twisting motion inside the pillar but then the minus microtubules suddenly slide off of the plus ones, finally lying close to parallel with the plane of attachment.

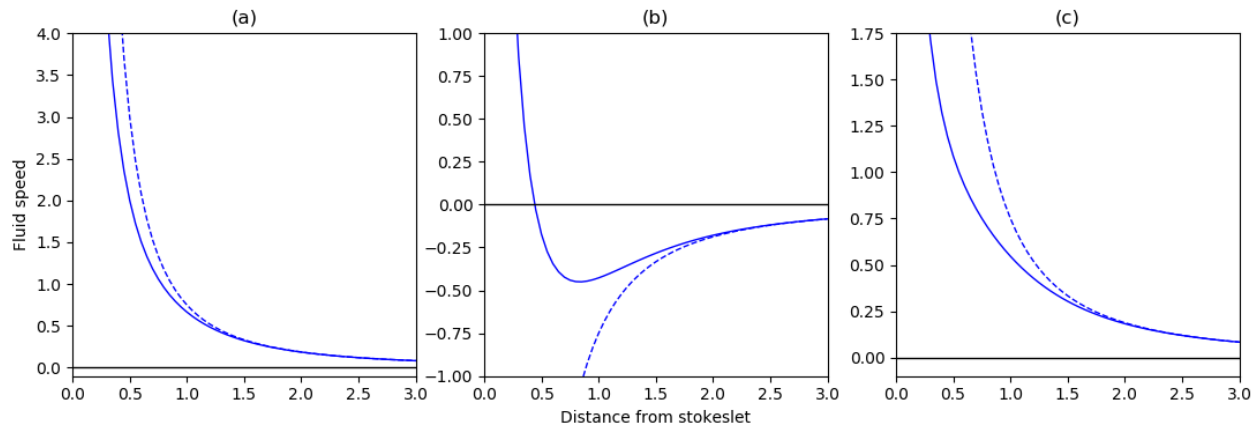


Figure S-1. Fluid speeds as a function of distance  $\rho$  from the stokeslet  $\mathbf{F} = \hat{i}$ . Solid curves are calculated using the full interaction tensor (S-2) and dashed lines are the far-field approximation (S-3). (a)  $u_x(\rho)$  along the line  $y = 0$ ; (b)  $u_x(\rho)$  along the line  $x = 0$ ; (c)  $u_y(\rho)$  along the line  $y = x$ .

## II. THE QUASI-2D INTERACTION TENSOR

The interaction tensor used in simulations is that of a stokeslet enclosed by two infinite parallel plates, as derived by Liron and Mochon[1]. In general, the interaction tensor  $\mathbb{G}$  is defined as the relationship between the fluid flow  $\mathbf{u}(\mathbf{r})$  and the stokeslet  $\mathbf{F}$  which causes this flow:

$$\mathbf{u}(\mathbf{r}) = \mathbf{F} \cdot \mathbb{G}(\mathbf{r}) \quad (\text{S-1})$$

We assume the system is embedded in a viscous fluid with viscosity  $\mu$ . For computational efficiency, we assume all monomers to be only in the  $xy$ -plane, with parallel plates at  $z = \pm H/2$ . This reduces a three-dimensional problem to two dimensions, as (a) the stokeslet is located in the  $xy$ -plane, (b) the stokeslet's direction has no  $z$ -component, and (c) we only concern ourselves with flows in the  $xy$ -plane (see Fig. S-2). For this arrangement, it can be shown from Liron and Mochon's general result that the interaction tensor a displacement  $\mathbf{r}$  (and  $\rho \equiv |\mathbf{r}|$ ) from a single stokeslet  $\mathbf{F}$  at the origin reduces to

$$\mathbb{G}(\mathbf{r}) = \frac{H}{8\pi\mu\rho^2} \left\{ \left[ 4 \left( \frac{\rho}{H} \right)^2 S_1 - \frac{1}{2} \frac{\rho}{H} I_1 \right] \mathbb{I} + \left[ 4\pi \left( \frac{\rho}{H} \right)^3 S_2 + \frac{1}{2} \frac{\rho}{H} I_1 - \frac{1}{4} \left( \frac{\rho}{H} \right)^2 I_2 \right] \frac{\mathbf{r} \otimes \mathbf{r}}{\rho^2} \right\} \quad (\text{S-2})$$

where

$$\begin{aligned} S_1 &\equiv \frac{1}{4} \sum_{n=0}^{\infty} \frac{(-1)^n}{\left[ \left( \frac{\rho}{H} \right)^2 + n^2 \right]^{1/2}} \\ S_2 &\equiv \frac{1}{4\pi} \frac{\rho}{H} \sum_{n=0}^{\infty} \frac{(-1)^n}{\left[ \left( \frac{\rho}{H} \right)^2 + n^2 \right]^{3/2}} \\ I_1 &\equiv \int_0^{\infty} \xi J_1 \left( \frac{\rho}{H} \xi \right) \frac{\tanh^2 \frac{\xi}{2}}{\sinh \xi - \xi} d\xi \\ I_2 &\equiv \int_0^{\infty} \xi^2 \left[ J_0 \left( \frac{\rho}{H} \xi \right) - J_2 \left( \frac{\rho}{H} \xi \right) \right] \frac{\tanh^2 \frac{\xi}{2}}{\sinh \xi - \xi} d\xi \end{aligned}$$

Here,  $J_n$  is the Bessel function of the first kind. Because  $S_1$  and  $S_2$  do not converge rapidly as defined above, we also make use of the Poisson sums

$$\begin{aligned} S_1 &= \sum_{k=0}^{\infty} K_0 \left[ \pi(2k+1) \frac{\rho}{H} \right] \\ S_2 &= \sum_{k=0}^{\infty} (2k+1) K_1 \left[ \pi(2k+1) \frac{\rho}{H} \right] \end{aligned}$$



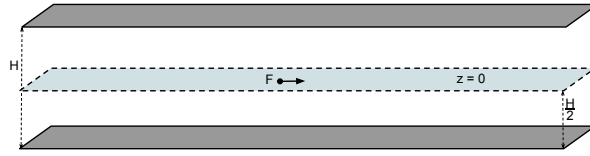


Figure S-2. Illustration of the geometry for which interaction tensor is derived in II. While this is a three-dimensional system, we constrain polymers to the  $xy$ -plane.

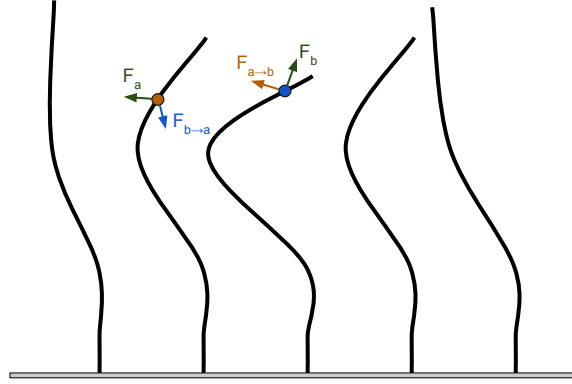


Figure S-3. Illustration of hydrodynamic forces between two example monomers in a planar polymer array. The green forces are the sum of non-hydrodynamic forces on the monomer (and by extension the force the monomer exerts on the surrounding fluid).  $\vec{F}_{a \rightarrow b}$  and  $\vec{F}_{b \rightarrow a}$  are the hydrodynamic forces on monomer  $b$  due to  $\vec{F}_a$  and the hydrodynamic force on monomer  $a$  due to  $\vec{F}_b$ , respectively.

where  $K_n$  is the modified Bessel function of the second kind.

In the far field, it can be shown that (S-2) approaches

$$\mathbb{G}(\mathbf{r}) \approx -\frac{3H}{32\pi\mu\rho^2} \left( \mathbb{I} - 2\frac{\mathbf{r} \otimes \mathbf{r}}{\rho^2} \right) \quad (\text{S-3})$$

Fig. S-1 shows plots of  $\mathbf{u}(\mathbf{r})$  at selected locations, and compares the exact value from (S-2) to the far-field approximation from (S-3).

We can now make some conceptual observations regarding this interaction tensor and how it compares to the boundary-free Oseen tensor  $\mathbb{G}_0$ :

$$\mathbb{G}_0(\mathbf{r}) = \frac{1}{8\pi\mu r} \left( \mathbb{I} + \frac{\mathbf{r} \otimes \mathbf{r}}{r^2} \right)$$

First, we immediately notice a  $1/r$  dependence (rather than  $1/\rho^2$ ). This means forces without boundaries tend to be more long-range, and boundaries result in long-range screening. Second,  $\mathbb{G}_0$  is always positive, whereas this is not true for the interaction tensor used here. One key implication of this is that flows created by a stokeslet are often flowing opposite its direction (e.g. Fig. S-1b). Both of these qualities may enhance metachronal behavior in the confined system. Screening means that interactions between nearby polymers are most important, creating a “domino effect” from one polymer to the next rather than having motion more influenced by long-range interactions. The creation of opposing flows means (among other things) that if one polymer is moving toward the anchoring surface, it may exert a force on many of its neighboring polymers *away* from the anchoring surface. This encourages wavelike behavior rather than uniformity of beating motion.

### III. SIMULATION METHODS

The algorithm we implement is built on work that was used to simulate the mechanism behind cytoplasmic streaming in *Drosophila* oocytes [2], and many of the methods and equations below are explained in detail in these papers. This software simulates an array of active microtubules tethered to a plane that works as follows and is explained in further detail below.

1. After an array of polymers is initialized, forces on all monomers are summed (described below, also see Fig. 1 of main paper) and monomer position and velocity are updated using time step  $dt$ .
2. This motion initiates complex flow in the surrounding fluid. The fluid flow is not simulated directly, but the resulting hydrodynamic forces from this flow are calculated via an Oseen tensor with corrections by Blake[3]. This is illustrated in Fig. S-3.
3. Forces on each monomer are summed, and monomer position and velocity are updated accordingly.
4. Once updated, steps 2-3 are repeated.

In the present work there were these differences:

1.  $N$  Microtubules are confined to the  $xy$ -plane, with polymer bases separated by a distance  $l$  tethered either to a flat plate at  $y = 0$  or to a circular boundary. For all presented results,  $N = 128$ . The geometry of this is shown in Fig. S-2.
2. At the tethering point, a potential was added in order to keep the base monomer approximately orthogonal to the boundary.
3. Rather than the Blake correction to the Oseen tensor, we use the simplified Liron/Mochon interaction tensor described in supplemental Section II. We also investigated varying the hydrodynamic coupling parameter  $k_{oseen} \equiv 1/(8\pi\mu)$ .

Now we describe how the above was accomplished in more detail. Each polymer is composed of  $n = 16$  monomers. The  $i$ th monomer position  $\mathbf{r}_i$  is updated using a fourth order Runge Kutta integration of the equation

$$\frac{d\mathbf{r}_i}{dt} = \mathbf{u}(\mathbf{r}_i) - k_{kin} (\mathbf{r}_{i-1} - \mathbf{r}_{i+1}) \quad (\text{S-4})$$

where  $dt$  is the time step (set to 0.003),  $k_{kin}$  (set to 0.2) controls the strength of the kinesin force tangent to the polymer ( $\mathbf{F}_{kin}$  in Fig. 1), and  $\mathbf{u}(\mathbf{r}_i)$  is the fluid velocity due to the motion of all other monomers as given by Equation S-1 and S-2 (which imparts the forces  $\mathbf{F}_{a \rightarrow b}$  in Fig. S-3):

$$\mathbf{u}(\mathbf{r}_i) = \sum_{j \neq i} \mathbf{F}_j \cdot \mathbb{G}(\mathbf{r}_i - \mathbf{r}_j) \quad (\text{S-5})$$

Here,  $\mathbf{F}_j$  is the total force on the fluid due to the  $j$ th monomer. Because there are no inertial effects when  $Re \ll 1$ , any non-hydrodynamic force exerted on the monomer must be transferred to the fluid. In our case,

$$\mathbf{F}_j = \mathbf{T}_j + \mathbf{C}_j + \mathbf{Q}_j, \quad (\text{S-6})$$

where

- $\mathbf{T}_j = k_{spr} [ (|\mathbf{r}_{j-}| - \ell) \hat{\mathbf{r}}_{j-} + (|\mathbf{r}_{j+}| - \ell) \hat{\mathbf{r}}_{j+} ]$   
with  $\mathbf{r}_{j\pm} \equiv \mathbf{r}_{j\pm 1} - \mathbf{r}_j$ , is the spring force keeping monomer separation approximately constant. For our simulations,  $k_{spr} = 100$  and  $\ell = 1$ . In these simulations the separation between polymer bases defines above,  $l$  is equal to  $4\ell$ .
- $\mathbf{C}_j = k_{stiff} (2\mathbf{r}_i - \mathbf{r}_{i+2} - \mathbf{r}_{i-2})$   
is the stiffness force which resists polymer bending.  $k_{stiff}$  is varied in our simulations, but typically  $5 \leq k_{stiff} \leq 20$ .
- $\mathbf{Q}_j = \mathbf{P}_j + \mathbf{B}_j + \mathbf{W}_j + \sum_k \mathbf{H}_{jk}$   
is the sum of miscellaneous conditional forces:

- $\mathbf{P}_j = k_{pin} (\mathbf{r}_j - h\hat{\mathbf{j}})$  if  $(j \bmod n) = 1$   
 is the force on the base monomer of each polymer chain keeping it pinned to the anchoring surface. For our simulations, we set  $k_{pin} = 100$  and  $h = 1$ .
- $\mathbf{B}_j = k_{pin2} (\mathbf{r}_j - \mathbf{r}_{j-1} - \ell\hat{\mathbf{j}})$  if  $(j \bmod n) = 2$   
 is the force on the second monomer in each polymer chain, keeping the base of each polymer approximately orthogonal to the anchoring surface ( $F_{base}$  in Fig. 1). For our simulations, we set  $k_{base} = 100$ .
- $\mathbf{W}_j = k_{wall} \left[ 1 - \left( \frac{d_{wall}}{y_j} \right)^4 \right] \hat{\mathbf{j}}$  if  $y_j < d_{wall}$   
 is the repulsive force exerted by the anchoring plane on any monomer that gets close to the wall. For our simulations, we set  $d_{wall} = 0.5$  and  $k_{wall} = 100$ .
- $\mathbf{H}_{jk} = k_{rep} \left[ 1 - \left( \frac{d_{rep}}{|\mathbf{r}_j - \mathbf{r}_k|} \right)^4 \right] (\mathbf{r}_j - \mathbf{r}_k)$  if  $|\mathbf{r}_j - \mathbf{r}_k| < d_{rep}$   
 is the repulsive force between monomers that are very close to one another. For our simulations, we set  $d_{rep} = 0.5$  and  $k_{rep} = 1$ .

#### IV. ANALYSIS OF UNIPOLARITY

The work of Sanchez et al. [4, 5] consists of a mixture of biotin-labeled kinesin-1 motors bound together to form clusters using multimeric streptavidin and taxol stabilized microtubules in a polyethylene-glycol solution with ATP. These form bundles of microtubules, some of which are adsorbed to air-water or air-glass interfaces, that point out from the interface forming a lawn of microtubule bundles. These bundles are flexible and show bending similar to what is seen in the simulations described here in both the time scales, length scales, and correlations between different bundles.

The question that is not answered in the experimental work is the directionality of the microtubules inside a bundle. The microtubules forced into bundles by the polyethylene glycol (PEG) could be of mixed polarity so that some have their minus ends at the interface while others have their plus ends there. We will refer to microtubules with different orientations as having different “polarities”, minus-ends against the interface as “minus” and those with opposite polarity as “plus”.

The problems with having a mixed polarity bundle are two fold. The first is that for a wide range of experimental parameters, we expect mixed polarity bundles to be unstable [6, 7]. The second problem is that it is not clear that mixed polarity bundles can give rise to the motion seen experimentally. We will analyze both problems below.

##### A. Instability of mixed polarity bundles

The first problem is that adjacent microtubules with different polarities will be linked by kinesin clusters that will apply equal and opposite forces to them. This will cause the minus microtubules to be pushed toward the interface, and the plus ones away from it. The forces from the kinesin act in parallel on a microtubule over its length which is of order  $10\mu m$ . The forces that these cause can be competitive with depletion forces caused by the PEG as we will now see. A full analysis of this is not possible without more information about the details of the system such as the density of kinesin clusters and chain lengths of the PEG. However we can do a calculation to show that even with very modest assumptions concerning kinesin density, expulsion of plus microtubules will take place.

Depletion forces exert an osmotic pressure on microtubules and filaments. Each polymer excludes a roughly spherical region of order its radius of gyration  $R_g$ . Entropic forces favor the separation of microtubules into bundles because less volume is excluded by the PEG. We will estimate the force acting on a single microtubule protruding from a bundle. PEG is depleted in a region of size  $R_g$  around the microtubule. The increase in free energy per unit area caused by this depletion is of order  $pR_g$  where the osmotic pressure is  $p = k_B T \rho$ , and  $\rho$  is the number of polymers per unit volume. The increase in free energy  $dF$ , in raising the microtubule by a height  $dz$ , is  $dF = (2\pi R_m dz) p x$ . Here  $R_m$  is the microtubule radius. If we assume that the polymers are close-packed around the microtubule to get the maximum effect, then  $\rho = 1/(4\pi R_g^3/3)$ . So the force needed to push the microtubule out of the tip of the bundle is  $f = dF/dz = (3/2)R_m k_B T / R_g^2$ .

$R_m \approx 13nm$  and conservatively taking  $R_g = 1nm$ , which is quite small for PEG,  $f = 81pN$  The stall force of kinesin is approximately  $5pN$  [8]. So only 16.2 kinesins are needed to overcome the depletion forces and expel this microtubule from the bundle.

The minimum separation of kinesin on a microtubule is  $8nm$  and there are 13 tracks around its circumference. Because kinesin has a strong affinity for microtubules we expect a high density of bound kinesin. Therefore 16 kinesins contributing to the force over a distance of  $10\mu m$  is over three orders of magnitude less dense than the maximum density attainable. This suggests that for a wide range of parameters, the microtubule bundles will become unipolar with minus-ends against the interface.

## B. Model of mixed polarity bundles

The second problem is that it is not clear that a mixed polarity bundle can give rise to the motion seen in experiment. Here we analyze this possibility by using simulation methods similar to what was used previously to understand molecular motor dynamics [9]

We assume that the microtubules are inextensible and that opposite polarity microtubules apply forces in equal and opposite directions. We discuss the different forces separately.

First there is an effective attractive interaction between microtubules independent of their polarities induced by the presence of PEG polymers. We choose a short range force so the monomers separated by a distance  $\mathbf{r}$  within a range  $\sigma_s$  will feel an attractive force due to depletion forces as discussed above. To simplify the expressions we use a normalized unitless distance  $\Delta \equiv \mathbf{r}/\sigma_s$ . The force between any two monomers for  $\Delta < 1$  is taken to be

$$\mathbf{f}_{attr} = f_a \Delta^4 (1 - \Delta^{12})^3 \mathbf{r} \quad (\text{S-7})$$

where  $f_a$  is the strength of the attractive interaction. The reason for choosing this functional dependence on  $\Delta$  was to produce a force that was close to constant for  $\Delta < 0.6$ , and then drop smoothly to zero, so as to work well with the Runge Kutte algorithm.

Second, we introduce an even shorter range repulsion between monomers that diverges at a hard core radius  $\sigma_h$  and goes to zero at  $\sigma_s$ :

$$\mathbf{f}_{rep} = f_r \left( \frac{1}{r^2 - \sigma_h^2} - \frac{1}{\sigma_s^2 - \sigma_h^2} \right)^4 \mathbf{r} \quad (\text{S-8})$$

where  $f_r$  is the strength of the repulsive interaction.

Third, we introduce an equal and opposite forces between monomers on opposite polarity microtubules that are within a distance  $\sigma_s$ . The direction of the force is as follows. We compute the tangents to both monomers as  $(\mathbf{r}_{i+1} - \mathbf{r}_{i-1})/2$ . Then we choose the direction  $\mathbf{t}$ , to be the average of these two tangents. The magnitude of the kinesin force is

$$\mathbf{f}_{kin} = f_k (1 - \Delta^{12})^3 \quad (\text{S-9})$$

where  $f_k$  is similar the symbol used previously in the main text and denotes the magnitude of the kinesin force.

These forces are added to the elastic forces, viscous drag, and tension that must be introduced to conserve link length and the equation of motion is iterated using a method for updating chains with constant link length [10, 11].

We also tried two separate kinds of boundary conditions. First, tethering the chains to fixed points on the surface which we will call “fixed” boundary conditions. Second, confining the chain ends to a two dimensional plane but letting the ends move within that plane, which we will call “sliding” boundary conditions.

We tried a wide range of parameters, of different elastic constants, attractive interactions, number of microtubules, and boundary conditions. What we found is now summarized.

For two chain bundles of opposite polarity we did find a set of parameters which showed movement of the bundle with:  $f_r = 10.0$ ,  $\sigma_s = 2$ ,  $\sigma_h = 1$ ,  $f_a = 3$ ,  $f_k = 0.2$ ,  $k_{stiff} = 100$ , and chain length of 20, see supplemental movie S11.

For larger bundle sizes, e.g. 9 chains, we did not find anything similar to experiments. With fixed boundary conditions, and started as a pillar of parallel microtubules with slightly randomized directions, the chains would settle down to a pillar shape that would not change with time for sufficiently small attractive interactions  $f_a$ , but when this became greater than a certain value that depends on elastic constant and other parameters, it would suddenly collapse into a ball because this is more highly favored energetically.

When we chose sliding boundary conditions, and for sufficiently weak attractive interactions,  $f_a = 1$  there was a regime where there was twisting motion inside the pillar but then the minus microtubules would suddenly slide off of the plus ones, finally lying close to parallel with the plane of attachment, see supplemental movie S12. It therefore

appears that a two microtubule bundle moves because of a strong anisotropy in forces seen in cross sections. In larger bundles, the forces through the bundle are more homogeneous which acts to stabilize them.

We conclude that by direct physical modeling of a mixed polarity bundle, it is not clear if there are any reasonable parameters which show motion similar to what is seen in the experiments of Sanchez et al [4, 5].

Note that the elastic constant of a microtubule in a bundle will depend strongly on the rate at which it is bent. For very short times, the bonds between different microtubules caused by kinesin binding will be fixed in position giving the bundle the elastic constant of a cylinder of radius  $R$  which is  $\propto R^4$ . However the oscillations here take place on minute timescales. In that case the individual kinesin molecules have velocities of order  $1\mu\text{m}/\text{s}$  so they unbind and move very far on this time scale. This allows neighboring microtubules to move relative to each other, to eliminate stress. Therefore on sufficiently long timescales, this reduces the elastic constant of a microtubule to that of one in isolation.

- 
- [1] N. Liron and S. Mochon, *Journal of Engineering Mathematics* **10**, 287 (1976).
  - [2] C. E. Monteith, M. E. Brunner, I. Djagaeva, A. M. Bielecki, J. M. Deutsch, and W. M. Saxton, *Biophys. J.* **110**, 2053 (2016).
  - [3] J. R. Blake, *Mathematical Proceedings of the Cambridge Philosophical Society* **70**, 303 (1971).
  - [4] T. Sanchez, D. Welch, D. Nicastro, and Z. Dogic, *Science* **333**, 456 (2011).
  - [5] T. Sanchez and Z. Dogic, in *Methods in enzymology*, Vol. 524 (Elsevier, 2013) pp. 205–224.
  - [6] K. Kruse and F. Jülicher, *Physical Review Letters* **85**, 1778 (2000).
  - [7] T. B. Liverpool and M. C. Marchetti, *Physical Review Letters* **90**, 138102 (2003).
  - [8] E. Meyhöfer and J. Howard, *Proceedings of the National Academy of Sciences* **92**, 574 (1995).
  - [9] J. M. Deutsch and S. E. Martin, *Macromolecules* **48**, 6703 (2015).
  - [10] J. Deutsch, *Science* **240**, 922 (1988).
  - [11] J. Deutsch and T. Madden, *The Journal of Chemical Physics* **90**, 2476 (1989).